PCCP

Accepted Manuscript

ROYAL SOCIETY OF CHEMISTRY

www.rsc.org/pccp

PCCP

Perspective

Progress towards high-power Li/CFx batteries: Electrode architectures using carbon nanotubes with CFx

Received 00th January 20xx,
Accepted 00th January 20xx

DOI: 10.1039/x0xx00000x

www.rsc.org/

Qing Zhang,[a] Kenneth J. Takeuchi,[a, b]* Esther S. Takeuchi,[a, b, c]* and Amy C. Marschilok[a, b]*

Carbon monofluoride (CFx) has a high energy density, exceeding 2000 Wh/kg, yet its application in primary lithium batteries is limited by its power capability. Multi-walled carbon nanotubes (CNT‡) are appealing additives for high-power batteries, due to their outstanding electronic transport properties, high aspect ratio necessitating low volume fraction for percolation, and high tensile strength. This perspective describes the current state of the art in lithium-carbon monofluoride (Li/CFx) batteries and highlights opportunities for development of high-power Li/CFx batteries via utilization of carbon nanotubes. In this report, we generated several electrode architectures using CFx/CNT combinations, and demonstrated the effectiveness of CNT in enhancing the rate capability and energy density of Li/CFx batteries. First, we investigated the resistivity of CFx combined with CNT and compared the CFx/CNT composites with conventional carbon additives. Second, we built CFx-CNT electrodes without metallic current collectors using CNT as substrates, and compared their electrochemical performance with conventional CFx electrodes using aluminum foil as a current collector. Further, we fabricated multi-layered CNT-CFx-CNT composite electrodes (sandwich electrodes) and studied the impact of the structure on the performance of the electrode. Our work demonstrates some of the opportunities for utilization of CNT in CFx electrodes and the resultant implementation of CFx as a battery cathode in next-generation high-power batteries.

1 Introduction

1.1 Development of Li/CFx batteries

The utilization of CFx as cathode material in lithium primary batteries was first reported in 1970s by Watanabe et al. from Matsushita Electric Industrial Company in Osaka, Japan.[1, 2] Refinements were reported in 1981 by Toyoguchi et al.[3] CFx is the notation for poly carbon monofluoride. CFx compounds can be non-stoichiometric with x varying between 0 - 1.3,[4, 5] and most CFx used in lithium batteries has x around 1. CFx materials are usually prepared by fluorination of graphite, petroleum coke, carbon fibers and other carbon sources. Carbon precursor and reaction conditions affect the properties and electrochemical performances of product.[6] The crystal structure of CFx compound with x > 0.5 was investigated by several groups.[7, 8] Nakajima et al. first proposed that CFx has two phases: CF_1 and $CF_{0.5}$.[9] In the CF_1, fluorine atoms are intercalated between every carbon layers to generate a CFCF stacking sequence, while in the $CF_{0.5}$, fluorine atoms are intercalated in every other layer of carbon atoms to yield a CCFCCF stacking sequence. Both phases have hexagonal symmetry. CFx is described as a mixed phase material when x is between 0.5 and 1. When x is between 1 and 1.3, the material consists primarily of CF_1 phase with additional -CF_2 surface groups.[10] The nature of C-F bonding changes from ionic to semi-ionic or semi-covalent to covalent with increasing F content.[11-14] As x approaches 1, C-F bonding is covalent and the material becomes totally insulating. The C-F bond length decreases from 0.3 nm when the bonding is ionic to 0.141 nm when bonding is covalent.[5] The inherently poor electrical conductivity is the cause for several shortcomings of the Li/CFx batteries, including limited rate performance, voltage delay during the initial discharge process, and heat generation accompanying the discharge process.[15]

A commercial Li/CFx battery (as shown in **Figure 1**) is constructed with a composite cathode consisting of CFx, a conductive additive and a polymeric binder, a lithium anode, a polypropylene separator and a non-aqueous electrolyte (such as $LiBF_4$ in γ-butyrolactone).[16] The overall discharge reaction of the Li/CFx battery can be expressed as "$CF_x + xLi \rightarrow C + xLiF$".[15] It has been shown that the electrochemical discharge product is an intermediate phase consisting of carbon, fluoride ions, and a solvated lithium ion.[17, 18] The discharge reaction can also be considered as "$CF_x + xLi + xS \rightarrow C(Li^+SF^-)_x$" where S represents solvent molecules coordinated with each Li^+ ion.

[a] Department of Materials Science and Engineering, Stony Brook University, Stony Brook NY, 11794.
[b] Department of Chemistry, Stony Brook University, Stony Brook NY, 11794.
[c] Energy Sciences Directorate, Brookhaven National Laboratory, Upton NY, 11973.
*Corresponding authors: kenneth.takeuchi.1@stonybrook.edu (KJT), esther.takeuchi@stonybrook.edu (EST), amy.marschilok@stonybrook.edu (ACM)

† Footnotes relating to the title and/or authors should appear here. Electronic Supplementary Information (ESI) available: [details of any supplementary information available should be included here]. See DOI: 10.1039/x0xx00000x

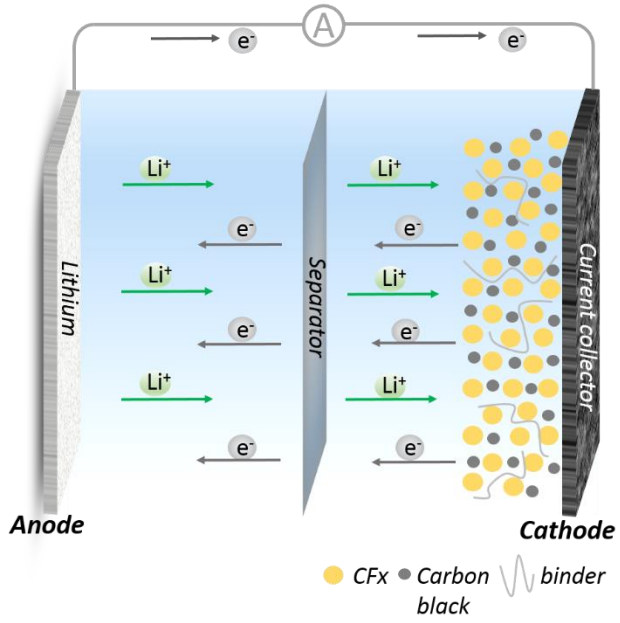

Figure 1. Schematic of a Li/CFx battery.

Upon formation, the intermediate product subsequently decomposes into the final discharge products: "$C(Li^+SF^-)_x \rightarrow C + xLiF + xS$".[17, 18] Based on the discharge reaction, the specific capacity of CFx material is related to the x value. The theoretical capacity of CFx is 865 mAh/g when x equals to 1, and the specific capacity decreases as the x value decreases.[9, 19]

The thermodynamically determined open circuit potential (OCV) of Li/CFx (x = 1) batteries is 4.57 V. In most non-aqueous liquid electrolyte, CFx cathode has a measured OCV of 3.2 V vs. Li. The difference between the theoretical and measured OCV values can be attributed to several factors. Reaction of CFx with solvent, and the slow formation and decomposition of intermediate phase has been proposed to be a dominant factor.[20-23] Smaller electrolyte solvent molecule size leads to lower lithium solvation energy, therefore the lithium ion is solvated more strongly and shows lower ability to pair with fluoride ion, leading to higher overpotential. Solvents like dimethylsulfoxide and γ-butyrolactone show higher overpotential than propylene carbonate and sulfolane when used as electrolyte solvents.[23] The overpotential of CFx has also been related to its fluorine (x) content, as material of higher fluorine content has a larger interlayer spacing, which may facilitate lithium ions migration.[18] Additionally, when the lattice of the starting carbon material exhibits a curvature as is the case for carbon nanotubes and fullerenes, the C-F bonding nature after fluorination as well as discharge potential can be influenced by the curvature. Higher curvature causes weaker covalent bonding so that the discharge potential is higher (overpotential is reduced).[24, 25]

Simulation of the Li/CFx system with constant load resistance proved that the system obeys Tafel kinetics at low discharge rates, and the transport processes such as concentration variations in solid and liquid phase are of negligible importance due to low kinetic rates.[26] The electrochemical reaction is confined to the carbon/CFx interface, and the OCV of the cell has been reported to depend of the nature of the starting carbon and processing temperature to produce CFx, as suggested above. During constant-current discharge, there is a relatively constant cell resistance over the majority of the discharge, but a rapid decrease in first 5% (resulted from carbon generation) and last 15% to 20% of discharge (resulted from available reduction of active area).[26] Simulation of pulse discharge of the Li/CFx system suggests that carbon generation during the initial discharge period results in a significant capacitance which slows the potential response to interruption in load. The cathode plays a dominant role in resistance of the cell, therefore increases in cathode thickness and coverage of CFx with LiF and changes in contact among cathode particles may lead to changes in cell resistance as a function of discharge.[27]

It has been widely accepted that the reaction of CFx with lithium is irreversible and Li/CFx batteries cannot be recharged. However, it is noteworthy that the reversibility of CFx in sodium ion batteries was demonstrated in 2014 by Liu et al. Unlike LiF which cannot be electrochemically decomposed, NaF can be reversibly decomposed in the reaction with carbon at the voltage range from 1.5-4.4 V. A reversible discharge capacity of 786 mAh/g was achieved and the high reversibility of CFx with Na was demonstrated, illustrating that CFx is also a promising cathode material for rechargeable sodium batteries.[28]

1.2 Applications of Li/CFx batteries

Implantable cardiac pacemakers Depending on the power level, implantable medical device primary batteries fall into several categories: low-rate batteries outputting microwatts of power such as batteries for cardiac pacemakers and hearing devices; medium-rate batteries outputting milliwatts of power such as batteries for drug delivery systems and bone growth stimulators and high-rate batteries such as batteries for implantable cardiac defibrillators which need to deliver a power pulse of 40 J within milliseconds.[29] Among all of the applications, reliability, predictability, and long shelf-life are essential requirements for implantable biomedical device batteries, where high energy density and lightweight are also important. By virtue of the light weight and high theoretical capacity of lithium metal, lithium primary batteries have been widespread in health-improving medical devices since the successful implantation of the first lithium-powered pacemaker in 1970s.[30, 31]

Li/CFx battery has been a commercially viable technology for implantable cardiac pacemakers since it was proven to be a reliable power source for advanced pacemakers in 1996.[32] A cardiac pacemaker is a medical device that can help control abnormal heart rhythms. It delivers electrical pulses with proper intensity to stimulate the heart to beat at a desired rate. Surgical treatment is required to implant a cardiac pacemaker.

The first cardiac pacemaker powered by a zinc/mercuric oxide battery was successfully implanted in a human being in 1960s.[33, 34] This battery system helped make possible the implantation of the pacemaker, but notable drawbacks such as high self-discharge and generation of hydrogen as a by-product of cell reaction existed. A rechargeable pacemaker battery was developed in 1970s using a nickel/cadmium battery system. The battery was recharged inductively through the skin, however, the battery was short-life and patient compliance was difficult. Nuclear batteries were developed for pacemakers. These batteries used plutonium to generate heat and convert heat into electrical energy. However, the nuclear component was highly toxic once leaked into blood and tracking patients who were implanted with these devices was an issue.[35] Several lithium battery systems have been used in implantable cardiac pacemakers including lithium/iodine (Li/I_2), lithium/thionyl chloride ($Li/SOCl_2$), lithium/manganese dioxide (Li/MnO_2), lithium/cupric sulphide (Li/CuS) and lithium/silver chromate (Li/Ag_2CrO_4). [36,35,37,32] The electrochemical properties of these battery systems are listed in **Table 1**. Li/I_2 batteries have been a popular power choice in pacemaker batteries because of the high energy density and long shelf life since they were invented in 1970s.[38] The cathode of Li/I_2 battery is usually a mixture of iodine and poly(24-vinyl)pyridine (PVP), which reacts with a portion of iodine and makes the mixture conductive. The system contains a solid electrolyte which grows thicker as the cell is discharged, resulting in decrease in conductivity over discharge and limiting the rate performance of the battery.[39] While pacemakers have required power output in microwatt range historically, for modern devices which integrate new features like inductive and radiofrequency telemetry and programmability, requiring more capable and long-lasting batteries, Li/I_2 batteries are no longer the first choice.[32] Li/CFx batteries which were commercialized 30 years ago have become a rather more attractive candidate for pacemakers. The theoretical energy density for Li/CFx batteries is 2180 Wh/kg, which is about four times of Li/I_2 batteries. Li/CFx batteries usually have liquid electrolyte, therefore the internal resistance is lower than that of Li/I_2 system and remains unchanged most of the service life.[40] Furthermore, Li/CFx systems are compatible with titanium casing, which is about half the density of stainless steel, and density of CFx itself is lower than iodine, which gives Li/CFx battery systems a 50% reduction in weight compared with Li/I_2 battery systems while maintaining comparable volumetric energy density.[32, 41]

Furthermore, CFx materials have been mixed with other electroactive materials to combine their superior features to make hybrid batteries: A blend of CFx and MnO_2 provides higher rate capability than a CFx cathode, higher energy density than a MnO_2 electrode, excellent low temperature performance with no initial voltage delay.[42] The Li/CFx-MnO_2 systems can be utilized in higher rate applications such as remote metering and security alarm systems. A combination of CFx and $Ag_2V_4O_{11}$ (SVO) can provide both high power density and high energy density, where the CFx component contributes favourably to energy density and the SVO components contributes favourably to power density. The system was introduced to power devices for treating atrial fibrillation in 1999 and to power implantable pulse generators in 2000. Since then, this hybrid system has been used in other implantable devices such as cardiac pacemakers and drug-delivery devices.[45, 46]

Table 1. Comparison of Li/CFx batteries to other lithium primary batteries used in implantable medical devices.[43, 44]

Cell chemistry	Nominal cell voltage (V)	Theoretical capacity (mAh/g)	Theoretical energy density (Wh/kg)	Rate perform-ance
Li/I_2	2.8	211	591	Low
Li/CFx	2.8	865	2180	Low to medium
$Li/SOCl_2$	3.6	450	1470	Low to medium
Li/MnO_2	3.0	310	1005	Medium
Li/Ag_2CrO_4	3.1	160	515	Medium
Li/CuS	2.2	560	1050	Medium

Besides medical industries, Li/CFx batteries have been found in a wide range of applications in military, aerospace and electronic devices such as gas meters, cameras, computer clock and memory back-up which mostly require low-to-medium rates.[6, 47-50] Li/CFx cells exhibit the flexibility to be packed into different shapes such as spiral, coin, cylindrical and pouch based on the specific use. Extensive development on battery packing has been conducted to improve the overall energy density, where lighter materials such as aluminum and plastic are often used for packaging.[49, 51, 52] It is worth pointing out that Li/CFx batteries have become an attractive energy source for military applications due to their high energy density and reliable safety. With the Li/CFx technology, a BA-5590 lithium battery can be reduced to half the original weight while maintaining the same capacity. In addition to being used as portable power for long term missions, Li/CFx batteries also power electronics such as communication devices, GPS, surveillance, thermal imaging and detection equipment.[53]

1.3 Improving the power output of Li/CFx batteries

The operating discharge voltage of a Li/CFx cell is between 2.6-2.8 V due to the low electrical conductivity of CFx and the slow diffusion of solvated lithium ions in the intermediate phase.[54,55] As described before, the poor electrical conductivity results in several shortcomings of Li/CFx batteries, including limited rate performance, initial voltage delay in discharge process and heat generation accompanying the discharge process.[15]

Various approaches have been carried out to improve the poor electrical conductivity and enhance the rate capability of CFx material. Lam et al. have synthesized more conductive sub-fluorinated materials ($x < 1$) to improve rate performance. At low discharge rates (< 0.1 C), the energy density increases with fluorine content x. At higher rates (> 2.5 C), sub-fluorinated

compounds perform better than CFx (x > 1). The sub-fluorinated samples contain unreacted carbon, which could act as an intrinsic conductor between the fluorinated particles. However, this approach comes with a sacrifice in specific capacity.[56,4] Zhang et al. conducted a carbothermal treatment of the CFx material and carbon black with the presence of fluorinated polymer binder. The content of polymer affects the discharge performance of resulting product because of the catalytic effect of HF formed by the pyrolysis of the polymer on the decomposition of CFx and on the reaction of carbon black with the volatile fluorocarbons formed by the decomposition of CFx. The Li/CFx cell with the obtained CFx cathode showed 95 mV higher discharge voltage while maintaining the capacity.[57] Zhang et al. also developed a thermal treatment by heating a mixture of CFx and citric acid which could serve as extra carbon source. The discharge voltage was raised and cell resistance was lowered. [58] In both processes, sub-fluorinated CFx were produced so that the cathode resistivity was lowered. Another approach is to form a conductive coating on the surface of CFx particles to increase the exterior conductivity. Zhang et al. used carbon coating obtained by decomposition of PVDF in N_2 and a higher energy density and power density at higher discharge current rate (> 1 C) was observed.[59] Groult et al. electrodeposited polypyrrole on CFx particles in acetonitrile without affecting the structure of CFx core. The polypyrrole-coated CFx cathode can be applied high current up to 4 C while the discharge of pristine CFx is impossible at current higher than 1 C. With facilitated electrical conduction and contact between particles and collector, energy density and power density are tremendously increased.[60] A chemical approach developed by Nagasubramanian et al. was to add an anion-binding-agent to the electrolyte solution to dissolve LiF generated in the discharge reaction. Anion-binding-agent could dissolve LiF and prevent it from plugging the cathode pores and thus keep the bulk of the cathode accessible for further discharge reaction.[61] Rangasamy et al. presented a bifunctional electrolyte – Li_3PS_4. It can act as inert electrolyte at the anode site and as active component at the cathode site. The solid-state Li/CFx batteries can output 126.6% energy density beyond theoretical limit. The batteries also show good rate performance attributed to the improvement in lithium ion conductivity for the bifunctional electrolyte and better interfacial kinetics.[62]

The utilization of different nano-scale carbons as source materials for CFx production has also been investigated by researchers. Yazami et al. synthesized fluorinated carbon naofibres, which contained both fluorinated and un-fluorinated phase at nanometer scale. The un-fluorinated regions into the core could act as an electron transport path within the fluorinated structure and decrease the resistance. The fluorinated carbon nanofibres could sustain high current densities (6 C) and achieve high power density of > 8000 W/kg.[56] Jayasinghe et al. used CNT as fluorination carbon source because of the unique structure of CNT. Intercalation of fluorine creates defects on the tubes which could be additional paths for lithium ion diffusion. The existence of non-reacted carbon in the fluorinated CNT could promote electron flow and improve reaction kinetics.[63] Damien et al. found graphene a good choice for fluorination. The solvated lithium ions form layers of minimum thickness, which makes the transport faster and easier. Furthermore, the fluorine atoms situated on graphene surface are easily accessed by lithium ions compared to conventional CFx materials, leading to significant improvement in energy density and faradic yield. [64]

A mechanical approach of ball-milling to pre-treat the CFx material could reduce the particle size and alter physical and electrochemical properties. The volumetric energy density could be increased up to a factor of 3 with ball-milled particles compared to pristine material. The gravimetric energy density could increase up to a factor of 2 depending on discharge rates.[65]

It is important to realize that current collectors play a critical part in conducting electrons in the electrodes, especially for insulate materials like CFx. Yang et al. applied a novel graphene/Au composite as a current collector of CFx cathodes. With a rough and flexible surface structure favoring electron transfer, a high capacity of 653 mAh/g could be achieved at high current of 5 C. In contrast, CFx cathode on rigid aluminum foil failed at 1 C. [66] The findings provided a new strategy for designing CFx cathodes.

1.4 Use of multi-walled carbon nanotubes in batteries

CNT have become promising materials for both lithium primary batteries and rechargeable batteries on the grounds of their excellent electrical (10^6 to 10^7 S/m)[67] and thermal conductivity (>300 W/m•K),[68-70] chemical stability and mechanical flexibility.[70-72] They have been utilized in a variety of ways in batteries including conductive additive,[73] free standing anodes,[74] current collectors[75] and novel electrode structures such as layer-by-layer assembled electrodes.[76]

CNT as current collector CNT paper (buckypaper) is a thin sheet of aggregated CNT. CNT papers can be prepared by methods like casting CNT dispersions, physical blending with a binder,[77] spraying,[78] spin coating[79] and vacuum filtration et al.[74, 80, 81] The pore size of CNT paper can be tuned by changing the length of CNT.[82] The properties of CNT papers are not as good as individual CNT, and an important reason is that CNT are not aligning straight in a CNT paper. Alignment of CNT has been investigated to increase the mechanical strength and thermal and electrical conductivities.[83, 84] The electrical conductivity of CNT paper prepared by vacuum filtration can reach a conductivity of 1.0-5.0*10^4 S/m and a Young's modulus of 785 MPa.[67, 81, 83] CNT papers have attracted a lot of research attention as free-standing anodes for Li-ion batteries. CNT-based anodes exhibit reversible capacity in the range of 100-600 mAh/g depending on the preparation method, CNT structure and cycling conditions.[85, 86]

CNT as active component The chemical and physical properties of CNT can be tuned by changing surface conditions. It is

reported that surface functional groups on CNT such as oxygen and nitrogen can not only increase the capacitance of CNT,[87] but can go through Faradaic reaction to increase the gravimetric energy density as indicated by the potential-dependent gravimetric capacitance obtained from cyclic voltammetry measurements.[76] The reaction between Li^+ and carbonyl, ester and carboxylic groups takes place at an equilibrium voltage about 3.1-3.2 V vs. Li. The surface groups could impart more than 100mAh/g capacity to the electrode depending on processing parameters.[76, 88, 89] Recently it is reported that carbonyl (C=O) groups can be reduced by Li^+ and reversibly oxidized in the voltage range from 3.5 to 1.5 V vs. Li/Li^+ in aromatic carbonyl derivative organic materials.[90] Based on the research findings on the surface functional groups, we postulate that functionalized CNT could serve as an active component in the CFx cathode and contribute to the overall capacity, while boosting the conductivity of cathode.

CNT as conductive additive Conventional conductive additives used in batteries are mostly carbonaceous materials such as graphite and carbon black, the isolated single particle conductivity of which is in the order of 10^3 to 10^5 S/m.[91, 92] In comparison, CNT has conductivity in order of 10^6 to 10^7 S/m. Perfect CNT have similar conductivity as single-walled carbon nanotubes (SWCNT). The outer shell transports the electrons and contributes to final conductivity due to the coupling between the concentric layers.[93] To provide conductive pathways throughout an insulate electrode, a three-dimensional network needs to be formed by uniform distribution of conductive additive, which is known as percolation. Percolation threshold is characterized by a sharp drop in electrical resistivity with the increase content of conductive material. Controlling factors include aspect ratio, surface functional groups, alignment and dispersion state, as well as the nature of matrix material.[94-97,98] Conductive behaviour can also be changed if the conductive particles are packed in different ways, depending on the density, pressure and orientation.[67] With a high theoretical electrical conductivity and a high aspect ratio (ratio of length to diameter which is > 1000 typically), CNT can be seen as one-dimensional conductors generally,[99, 100] and can potentially establish a conductive percolation network with much lower mass loading than carbon black spherical particles and graphite flakes. On the other hand, the entanglement of nanotubes forms an open mesoporous network which provides a pathway for the ions to diffuse easily.[101] Work has been done investigating the influence of CNT as conductive additives in the matrix of $LiCoO_2$[102], $LiNi_{0.7}Co_{0.3}O_2$,[89] and $LiFePO_4$[73]cathodes, showing an approximately 10% improvement in reversible capacity of the electrodes compared to carbon black counterparts.

Aside from being used as fluorination carbon source, CNT are introduced into Li/CFx batteries by researchers as conductive additive. Li et al. replaced the conventional acetylene black with CNT and improved the rate capability of the Li/CFx cell.[103] At discharge rate of 1C, the specific capacity is improved by 26% when CNT are employed as conductive additive compared to same mass loading of acetylene black. To our knowledge, so far this is the only work that has been done regarding CNT functioning as conductive additives in Li/CFx batteries.

CNT dispersion The bottleneck of employing CNT as conductive additives is that CNT are held together in bundles by the strong Van der Walls interaction between tubes, and the high aspect ratio in combinations with the high flexibility leading to low efficiency on conducting electrons.[104] To disperse CNT in the matrix and effectively use the conductive pathways without diminishing electrical and mechanical properties remains a challenge for researchers. Physical methods of dispersion include ball-milling,[105, 106] shearing, ultra-sonication,[107] polymerization[108] and the use of surfactants,[107] and chemical methods including polymer-crafting and surface functionalization have been utilized by researchers.

Qian et al. developed a ultra-sonication-assisted solution-evaporation method to disperse CNT in polystyrene matrix homogeneously without destroying the structure of CNT.[109] Sandler et al. dispersed CNT in epoxy by pre-disentangling CNT in solvent with ultra-sonication, and then mixing with matrix resin by vigorous stirring.[110] Surfactants can be adsorbed onto CNT surface and render them soluble in aqueous solution or solvents. Unlike polymers which can also be used to disperse CNT, surfactants can be easily washed off. Therefore they are extensively applied in CNT dispersion. So far, various surfactants have been tried to disperse CNT or SWCNT, including sodium dodecyl benzenesulfonate (SDBS), dodecyltrimethyl-ammonium bromide (DTAB), hexadecyltrimethylammonium bromide (CTAB), octyl phenol ethoxylate (Triton X-100) and sodium dodecyl sulfate (SDS).[111,112,113-115] The dispersing power for each surfactant is intrinsic based on their chemical structures, and optimum CNT-to-surfactant ratio was found for several surfactants.[116] Concentration of surfactants should be sufficient enough to coat the surface of CNT.

CNT surface chemistry as well as the interaction between tubes can be altered by functionalization. CNT dispersion in liquid may be enhanced by choosing a specific type of surface functional groups. Acid treatment is a common way to purify, align CNT and attach oxygen functional groups to them (-C=O, -COOH, -OH).[117, 118] The amount of functional groups increases as treatment time increases. Ozone reacting with CNT produces ester and quinone functional groups.[119] Plasma polymerization of acetaldehyde and ethylenediamine vapors could activate CNT surface and introduce aldehyde (-CHO) and ($-NH_2$) groups.[120] Other functionalizations and polymer-grafting strategies are designed to make CNT soluble for different purposes.[121-125]

Each of the above technique has its pros and cons. It is reported that ultra-sonication results in fragmentation of CNT, which decreases the aspect ratio.[126] Ball-milling damages the tubes and creates amorphous carbon.[127] Chemical functionalization generates defects in lattice structure of carbon-carbon bonds and disrupts the extended π conjugation of CNT, consequently

reducing the electrical conductivity of CNT.[107, 128] There is a large variation in the reported percolation threshold on CNT dispersing in insulate matrix, which indicates that the dispersion state is affected by different processing parameters. It is critical to find the proper parameters which could give the system best dispersion state with minimum negative effects.

As we found in our work, there are practical issues related to CNT agglomeration and dispersion when they are blended with CFx material. No report has been found discussing how to tackle the problem of CNT agglomeration in CFx matrix when CNT do not wet well with CFx. In our work, the dispersion of CNT with CFx material has been investigated first. Since CFx material has the issue of low electrical conductivity and cathode swelling upon discharge,[129] CNT could serve as highly electrically conductive and flexible matrix, which not only provides good electrical contact for the whole electrode, but also effectively accommodate huge volume changes and dissipate heat generated during discharge. We incorporated CNT in the CFx electrode in two different parts: active material layer and current collector substrate. We demonstrated that the capacity, energy density and discharge rate capability could be greatly improved by incorporating CNT into the CFx electrode. We also designed novel sandwich-structure electrodes to eliminate the initial discharge voltage delay, which is one of the limitations of Li/CFx batteries. We carried out resistivity measurements on CFx material with different conductive additives and confirmed that CNT are advantageous in improving the CFx electrode conductivity.

2 Experimental

2.1 Materials sources and materials characterization

CFx and CFy materials (Advanced Research Chemicals. Co), multi-walled carbon nanotubes (Sigma-Aldrich) and super p Li* (TIMCAL) were used as received.

Particle size of materials was measured by a Horiba Laser Scattering Particle Size Analyzer. X-ray diffraction (XRD) was carried out with a Rigaku Smartlab X-ray Powder Diffractometer using Cu Kα radiation. Surface area measurement was done by the Brunauer-Emmett-Teller method. SEM images were taken on a JEOL 7600F Field Emission Scanning Electron Microscope. Resistivity of pellets was measured by a four-probe resistivity method. Microcalorimetry study was performed on a TAM III Microcalorimeter from TA Instruments.

2.2 Electrode fabrication, characterization, electrochemical test

CNT were dispersed, filtered and gently dried to form CNT papers. Cathode materials of certain formulations were coated on aluminum foil or CNT substrate.

To test material resistivity, CFx (CFy) material was mixed with conductive additives of certain percentages and polyvinylidene fluoride binder (PVDF) (5 wt. %). The mixture was pressed into pellets of 1.3 cm diameter by hydraulic press. The resistivity was tested by a four-probe resistivity method.

Conventional coin cells were assembled in a dry argon-filled glove box with lithium metal anode and the CFx-based cathode which has an active material loading of about 1.5 mg/cm^2. Cells were pulse-discharged and constant-current-discharged. In pulse-discharge, three different currents were applied to one cell, which were indicated in the form of "x/y/z mA/cm^2". X is the background discharge current, y is the lower pulse current and z is the higher pulse current.

3 Results and discussion

3.1 Characterization

Two CFx materials are investigated in this work, CFx and CFy. For both materials, the F/C elemental ratio was between 1 and 1.15. The carbon source of CFx is petroleum coke and that of CFy is carbon fiber. Both SEM images and Laser Particle Size Analyzer revealed that the particle size range of both materials is between 1 and 50 μm. CFy particles are longer in one dimension than CFx particles based on SEM images, as shown in **Figure 2**. The surface area measured by BET was 125 m^2/g for CFx and 283 m^2/g for CFy. **Figure 3** showed the XRD pattern of both materials and a schematic drawing assuming that CFx(CFy) has a hexagonal lattice structure like graphite. The first peak at 2θ=13° could be assigned to the (002) reflection, particular for compounds exhibiting high fluorine levels. The peak at 2θ = 41° could be assigned to (100) reflection, which is related to C-C bond strength (reticular distance of 0.214-0.221 nm).[130] However, due to peak broadening resulted from fluorination, it is questionable to assign the peaks to one phase.

Figure 4 is the SEM and optical images of CNT paper substrate as prepared. The raw MWCNT have a bulk density of 0.068 g/cm3 while the CNT paper has a density of around 0.3 g/cm3.

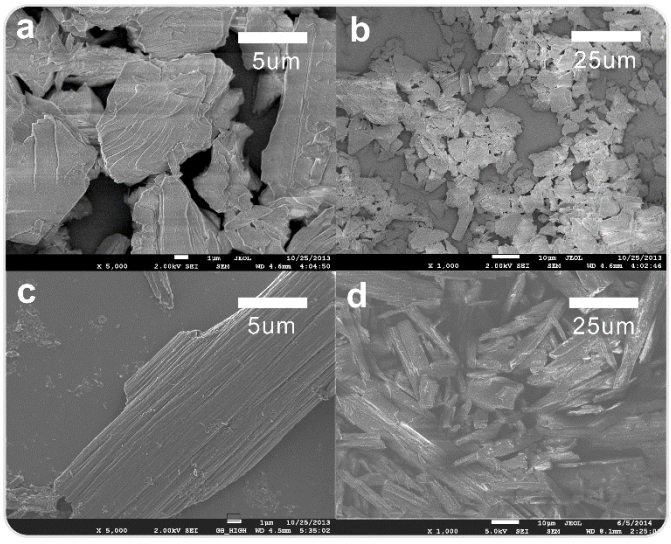

Figure 2. SEM images of CFx and CFy material. (a) CFx at 5 k magnification; (b) CFx at 1 k magnification; (c) CFy at 5 k magnification; (d) CFy at 1 k magnification.

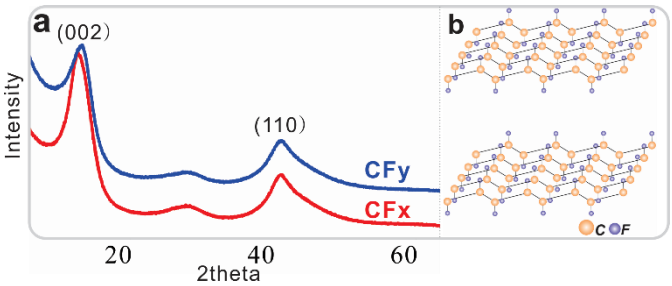

Figure 3. (a) XRD pattern of CFx and CFy material and (b) crystal structure of fluorinated carbon.

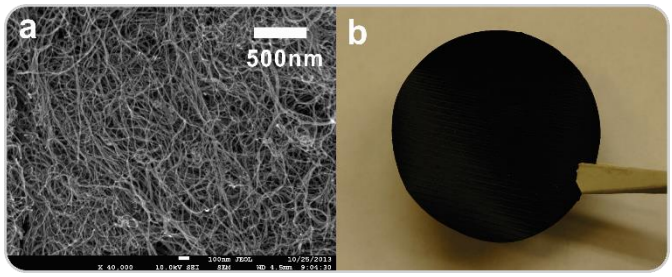

Figure 4. (a) SEM image and (b) optical image of CNT paper.

3.2 Material resistivity study and CNT as conductive additive

To study the mixing status of CFx (CFy) with super p and CNT with the same dry-mixing conditions (ball-milling), CFx (CFy) composite with 15 wt. % super p and CNT were mixed by plastic ball-milling, respectively. As revealed by the SEM images in **Figure 5(a-d)**, super p particles can disperse well in CFx **(a)** and CFy **(b)** matrix and CNT tend to entangle with each other **(c-d)**, which might lead to ineffective usage of CNT to form a conductive network. To get CNT to disperse better with CFx and CFy particles, higher energy steel ball-milling was employed to mix CNT with CFx and CFy. SEM images of the composite after steel ball-milling **(e-f)** showed that steel ball- milling did not improve the quality of CNT dispersion with CFx material (e), whereas it helped CNT disperse better with CFy material by dis-entangling the CNT bundles (f).

Composites of CFx with 8wt. % super p and CNT were used respectively to perform a time study to investigate the effect of ball-milling and optimal mixing time. As **Figure 6** shows, balling milling of 8min and 10 min CFx/CNT samples have significantly different resistivity. Ball-milling breaks the CFx particles and CNT, prompting larger contact area of CFx particles with CNT. However, longer ball-milling time may break CNT much shorter, which might result in poor overall conductivity. CFx/super p does not show as big a difference as CFx/CNT does in resistivity as time varies. Mixing time of 6 min gets the super p particles best dispersed with CFx particles considering the lower resistivity. Extended mixing time might cause the super p particles to aggregate, therefore the resistivity increases if mixing longer than 6 min.

To study the advantages of CNT over super p as a conductive additive, the resistivity of different mass loading of super p and CNT in CFx(CFy) composite was measured. The results are shown in **Figure 7 (a-b)**. For CFx **(a)**, at 5 wt. % of conductive additive, the resistivity of CFx/super p is nearly 10 times that of CFx/CNT. At 8 wt. % of conductive additive, CFx/super p still shows twice the resistivity of CFx/CNT. When the conductive additive is increased to 10 wt. %, CFx/super p and CFx/CNT show a similar resistivity level. As for CFy material **(b)**, when the conductive additive is 5 wt. %, the CFy/super p has a resistivity 30 times that of CFy/CNT. At 8 wt. % and 10 wt. % of conductive additive, the resistivity of CFy/super p is still nearly 10 times that of CFy/CNT. With the same mass loading, CFx(CFy)/CNT samples achieve much higher conductivity than CFx(CFy)/super p samples. The results suggest that less mass loading of CNT is needed than super p to form a conductive network. Both SEM images and resistivity tests results suggest that CNT dispersed

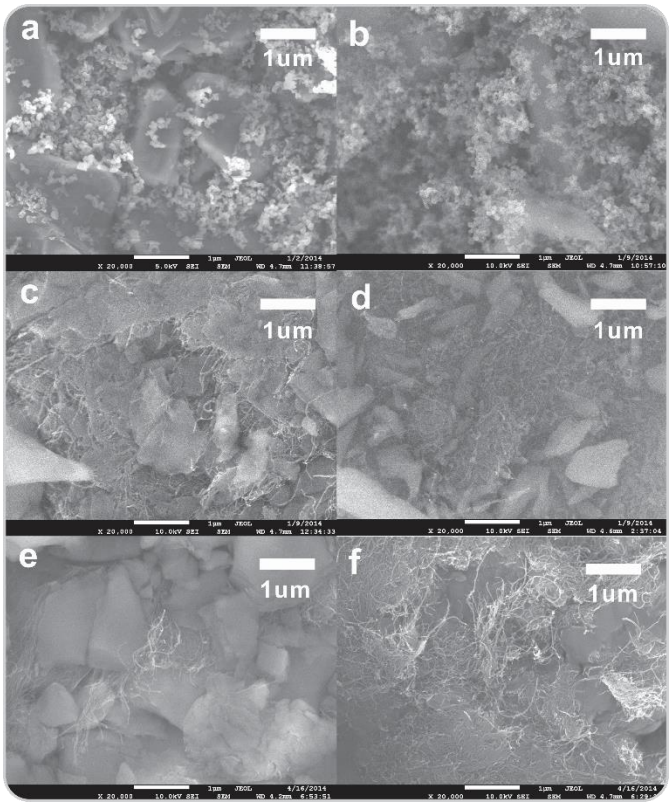

Figure 5. SEM images of (a) CFx/super P composite; (b) CFy/super P composite; (c) CFx/CNT composite; (d) CFy/CNT composite by plastic ball-milling; (e) CFx/CNT and (f) CFy/CNT composite by steel ball-milling.

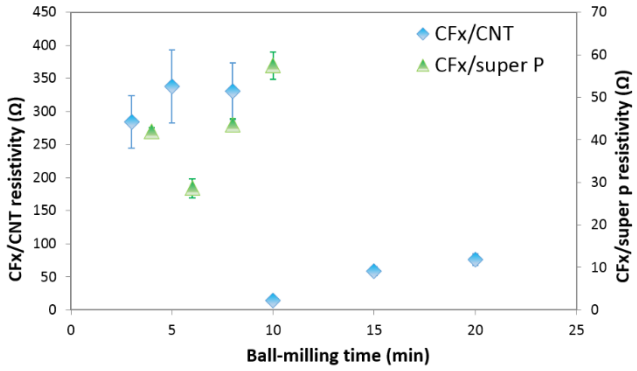

Figure 6. Resistivity of CFx mixed with both super p and CNT for different mixing time lengths.

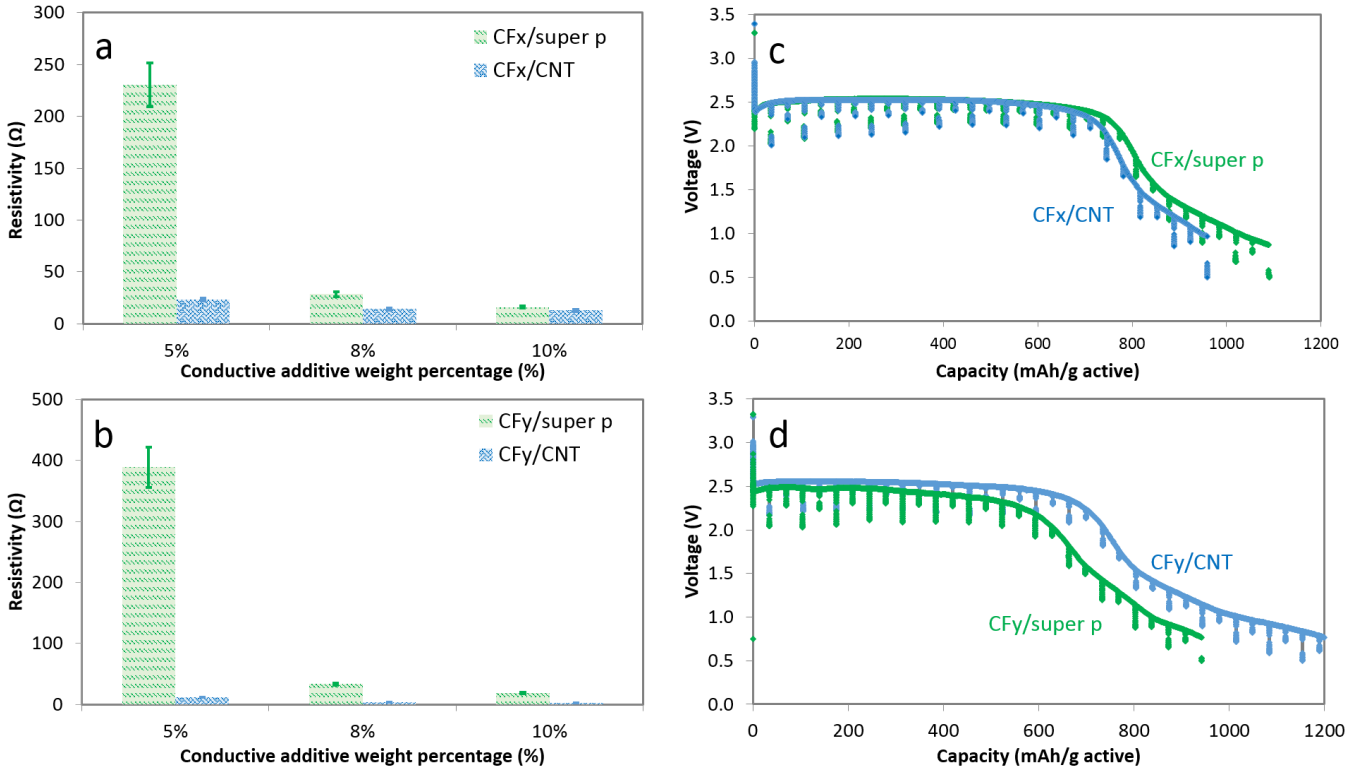

Figure 7. Resistivity of (a) CFx and (b) CFy mixed super p and CNT at different mass loading and pulse-discharge voltage vs. capacity plots of (c) CFx with 10 wt. % super p and CNT and (d) CFy with 10 wt. % super p and CNT at a current density of 1/4/8 mA/cm^2.

in CFy material are more effective in forming a conductive network, which proves that the nature of matrix material is an important factor affecting dispersion quality.

Corresponding electrochemical results were obtained by discharging the composite materials, as shown in **Figure 7 (c-d)**, at 10 wt. % of additives, for CFx material **(c)**, cells with CNT show a slightly lower initial voltage delay, but an approximately 50 mAh/g less capacity delivered compared with cells with super p. For CFy material **(d)**, cells with CNT show completely removed initial voltage delay, a higher discharge voltage and a 50 – 100 mAh/g more capacity compared with super p as conductive additive.

3.3 CNT as current collector

To select a suitable conductive additive for the following comparison of current collectors, electrodes with 80 wt. % active material (CFx or CFy), 15 wt. % conductive additives (super p, graphite or no additive) and 5 wt. % PVDF binder on CNT substrate were pulse-discharged. In **Figure 8 (a-b)**, discharge current density of 0.2/4/8 mA/cm^2 and 0.07/20/40 mA/cm^2 were applied and cells with different conductive additives are compared (Only results for CFx material are shown). At 0.2/4/8 mA/cm2, cells with super p show the highest background voltage: 2.52 V for CFx and 2.51 V for CFy. The cells with graphite show background voltage of 2.48 V for CFx and 2.46 V for CFy. The cells with no additives show lowest background voltage of 2.38 V for both CFx and CFy. At 0.07/20/40 mA/cm^2, cells with super p have the highest background voltage: 2.60 V for CFx and 2.57 V for CFy. Cells with graphite show lower voltage of 2.54 V for CFx and 2.56 V for CFy. Cells with no conductive additives show the lowest voltage of 2.49 V for both CFx and CFy.

Energy density for both groups of cells is shown in **Table 2**. For CFx at both discharge current densities, cells with super p exhibit the highest energy density. However, for CFy, cells with super p and graphite show comparable energy density at both discharge currents. At 0.07/20/40 mA/cm^2, cells with no conductive additives show even higher energy density, which is probably due to that discharge rate is low. However, from **Figure 8(b)**, it is obvious that the voltage drop during pulses is much deeper without conductive additives than that of the cells with super p or graphite.

Overall, compared to graphite and non-additive situation, super p is proved to be a more effective additive for pulse-discharge for both CFx and CFy material. So in the next step when we compare the substrates, we selected super p as conductive additive to improve the conductivity of the electrodes.

Same pulse-discharge and constant-current-discharge tests were performed on electrodes with both CNT substrate and Al foil as current collector at the same time. The electrodes used in this section have the composition of 80 wt. % CFx (CFy), 15 wt. % super p and 5 wt. % PVDF as binder.

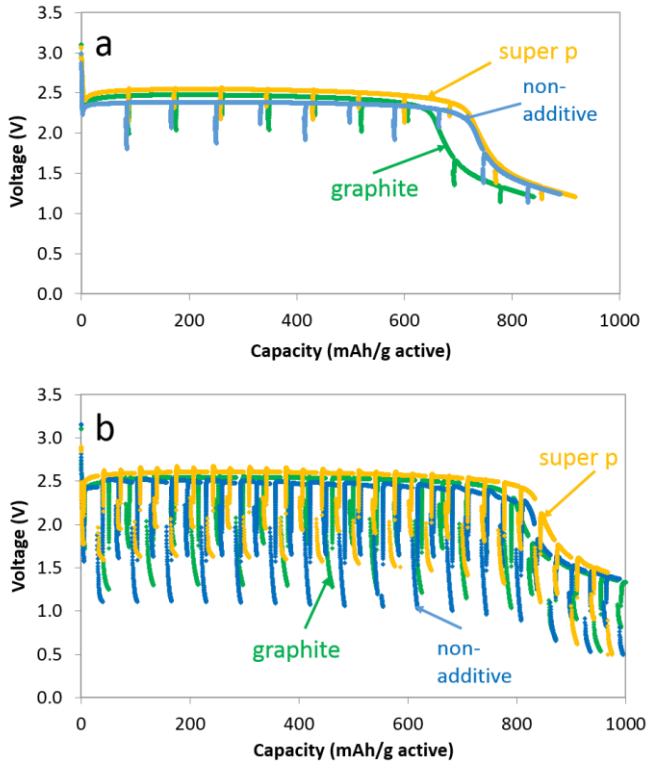

Figure 8. Pulse-discharge voltage vs. capacity plots of CFx material with super p, graphite and no additive at discharge current of (a) 0.2/4/8 mA/cm² and (b) 0.07/20/40 mA/cm².

Table 2. Energy density (Wh/kg of CFx or CFy material) of cells with different conductive additives.

	CFx (Wh/kg)		**CFy** (Wh/kg)	
Current (mA/cm²)	0.2/4/8	0.07/20/40	0.2/4/8	0.07/20/40
Super p	1842	2219	1636	1888
Graphite	1583	2061	1769	1890
Non-additives	1692	2073	1582	2016

Figure 9 is the discharge voltage vs. capacity plots of the electrodes on CNT substrate and Al foil at different current densities. As shown in **Figure 9 (a-c)**, cells with both substrates could discharge well when they are discharged at constant currents of 0.06, 0.3, 0.6 mA/cm². When the cells are pulse-discharged with higher current as shown in **Figure 9 (d-f)**, at current density of 0.2/4/8 mA/cm² **(d)** and 0.07/20/40 mA/cm² **(e)**, the Al foil cells have similar discharge profile as CNT substrate, despite that the voltage drops deeper than the CNT substrate. When the pulse current is increased further to 0.06/20/50 mA/cm² **(f)**, voltage of the cells with Al foil could not bounce back to normal discharge voltage after the first high-current pulse (50 mA/cm²), while the cells with CNT substrate could sustain the pulses maintaining the same background discharge voltage as constant-current-discharge cells with the discharge current of 0.06 mA/cm². The high-current pulses did not lower the back ground discharge voltage. CFy material has similar discharge profiles at these current densities applied which will not be shown here.

The group of cells of discharge current of 0.2/4/8 mA/cm² is taken to compare the voltage drop at individual pulse. **Figure 10** is the voltage respond at first three pulses for cells with CNT substrate and Al foil. Apparently, cells with CNT show a much lower voltage drop in all three pulses and have a different shape of pulse curve, which indicates a different kinetic of pulsing process.

Table 3 lists the specific capacity of cells with both substrates to 2 V and to 1 V. At lower discharge current of 0.06 mA/cm², cells with CNT substrate could deliver about 100 mAh/g more capacity than those with Al foil to 2 V and deliver twice the capacity of those with Al foil to 1 V. At other current densities, cells with CNT substrate show a 100 mAh/g higher capacity than those with Al foil. At 0.06/20/50 mA/cm² pulse-discharge when Al foil could not sustain, cells with CNT substrate still deliver about 440 mAh/g capacity.

Figure 11 lists the energy density with both Al foil and CNT substrate at each discharge condition. At each discharge current, CNT substrate cells display about 100-300 Wh/kg more energy density than Al foil cell. At discharge current of 0.06/20/50 mA/cm² which Al foil cell could not sustain, CNT substrate cells demonstrate a high energy density of 1124 Wh/kg for CFx material and 1101 Wh/kg for CFy material.

Table 3. Specific capacity (mAh/g of electrode) of cells with CNT substrate and Al foil at different discharge current densities.

Current (mA/cm²)	0.06		0.3		0.6	
Substrate	**CNT**	Al	**CNT**	Al	**CNT**	Al
Material			**CFx**			
Capacity at 2V (mAh/g)	**437**	342	**403**	303	**388**	315
Capacity at 1V	**963**	476	**541**	375	**495**	383
Material			**CFy**			
Capacity at 2V	**392**	283	**378**	285	**384**	290
Capacity at 1V	**1008**	358	**501**	349	**491**	358
Current (mA/cm²)	0.2/4/8		0.07/20/40		0.06/20/50	
Substrate	**CNT**	Al	**CNT**	Al	**CNT**	Al
Material			**CFx**			
Capacity at 2V	**392**	292	**385**	291	**427**	N/A
Capacity at 1V	**517**	372	**436**	306	**438**	N/A
Material			**CFy**			
Capacity at 2V	**371**	299	**318**	282	**393**	N/A
Capacity at 1V	**506**	370	**416**	289	**436**	N/A

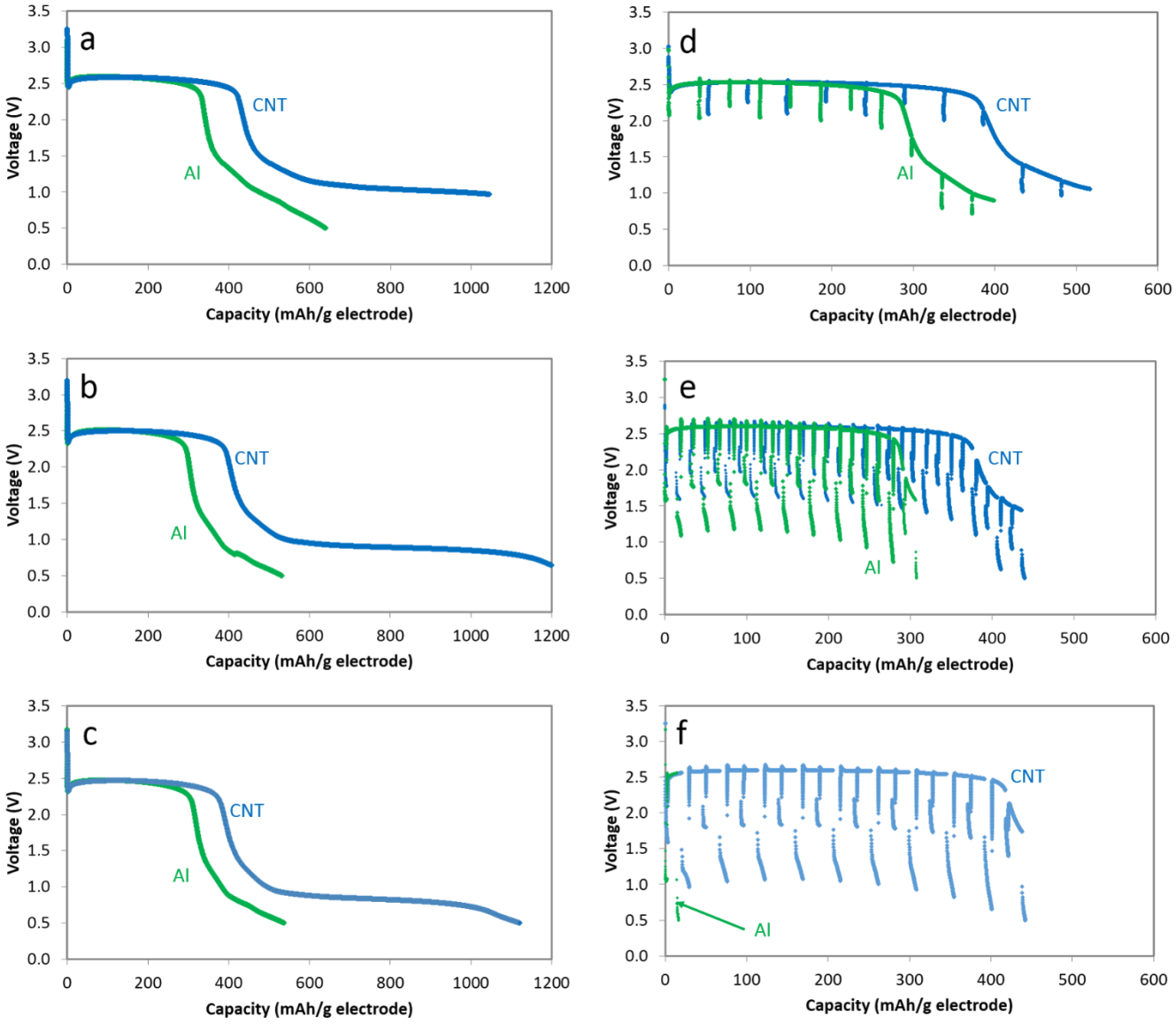

Figure 9. Comparison between CFx cells with Al foil and CNT substrate at current density of (a) 0.06 mA/cm^2; (b) 0.3 mA/cm^2; (c) 0.6 mA/cm^2; (d) 0.2/4/8 mA/cm^2; (e) 0.07/20/40 mA/cm^2 and (f) 0.06/20/50 mA/cm^2.

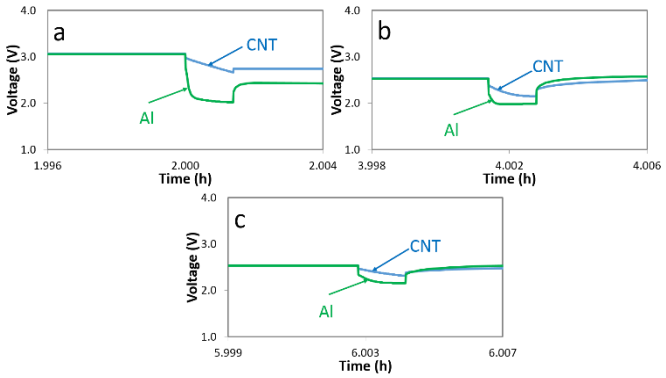

Figure 10. Comparison of the expansion of (a) first pulse of 4 mA/cm^2, (b) second pulse of 8 mA/ cm^2 and(c) third pulse of 4 mA/cm^2 of cells with Al and CNT substrate.

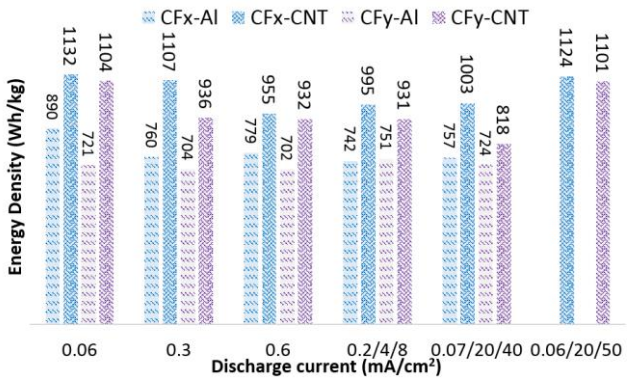

Figure 11. Energy density (Wh/kg of the electrode) of cells with CNT and Al foil substrate at different current densities.

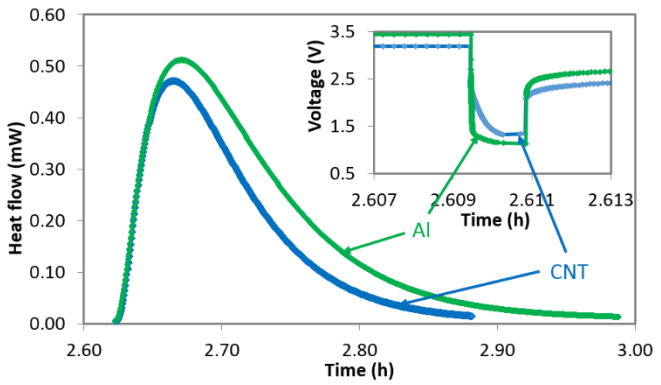

Figure 12. Heat flow of high current pulses of cells with Al foil and CNT substrate. The inset is the voltage profile of the current pulse of 40 mA/cm^2.

A microcalorimetry study was performed on both CNT substrate and Al foil based cells. The heat flow resulting from a 40 mA/cm^2 current discharge pulse for the two cells is shown in **Figure 12**. Microcalorimetry study on Li/CFx system has been previously reported by Read et al., involving a low current discharge test on the Li/CFx cell, where the thermal power after discharge was monitored in order to study the LiF formation process.[129] The goal of our microcalorimetry study was to examine the heat given off during high current discharge pulse and learn the effect of current collectors on heat generation of Li/CFx system. The 40 mA/cm^2 pulse was applied for 5 seconds (as indicated by inset in **Figure 12**), and heat generation started about 1 minute after the pulse was applied. Dissipation of the heat generated from pulse took about 20 minutes for each cell. The heat of the pulse monitored for the cells with CNT and Al foil substrates were 168 mJ and 227mJ, respectively. The CNT substrate showed less heat generation and maintained higher voltage during the pulse. The advantages the CNT substrate showed during the microcalorimetry measurement can be attributed to the 3D structure of CNT, resulting in better contact and the superior electrical and thermal conductivities which lead to lower polarization of electrode. Detailed analysis on heat generation will be fulfilled in future work.

3.4 Reduction of mass in CNT substrate

By virtue of the superior mechanical and electrical properties of carbon nanotubes, energy density could be further improved by reducing certain amount of carbon nanotubes while maintaining the electrochemical performance of the cell. **Figure 13** is a comparison between cells with CNT and reduced-mass CNT (R-CNT, mass reduced by 40%). **Table 4** gives the specific capacity and energy density improvement when the substrate dimension is reduced from CNT to R-CNT.

For CFx material, the capacity to 1 V is improved by 100 mAh/g and energy density is improved by 150 Wh/kg. For CFy material, the capacity to 1 V is improved by 120 mAh/g and energy density is improved by 250 Wh/kg.

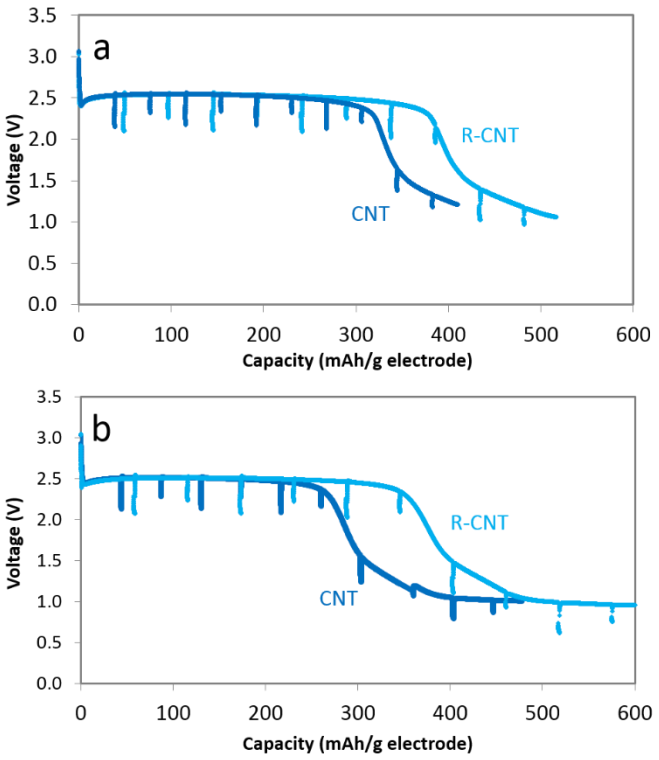

Figure 13. Discharge profile of (a) CFx and (b) CFy cells with CNT and R-CNT substrates.

Table 4. Specific capacity (mAh/g of electrode) and energy density (Wh/kg of electrode) of cells with CNT and R-CNT substrate.

	CFx		CFy	
	CNT	R–CNT	CNT	R–CNT
Capacity at 2 V (mAh/g)	330	392	283	371
Capacity at 1 V	410	517	478	504
Energy density (Wh/kg)	839	995	709	931

3.5 Sandwich-structure electrodes

To better take advantage of the superior conductivity of CNT and alleviate the initial voltage delay of Li/CFx battery discharge process, sandwich electrodes were fabricated by sandwiching a middle layer of of CFx(CFy) composite of two different formulations with two layers of CNT: One formulation is 15 wt. % CNT and 85 wt. % CFx (CFy) (Formula 1) and the other is 5 wt. % PVDF and 95 wt. % CFx (CFy) (Formular 2). A schematic graph of the sandwich-structure is shown in **Figure 14**.

Figure 14. Schematic graph of sandwich-structure electrodes.

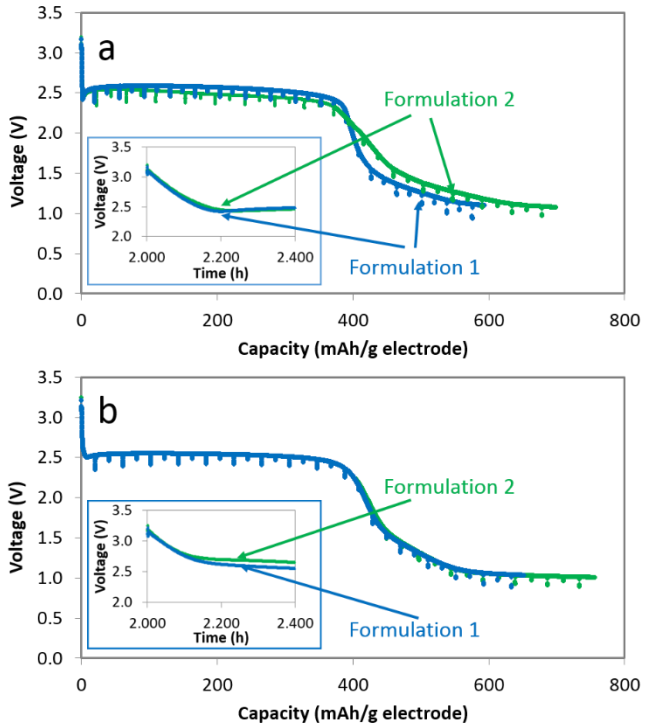

Figure 15. Discharge voltage vs. capacity plots of (a) CFx and (b) CFy sandwich-structure electrodes

The electrochemical discharge results are indicated in **Figure 15**: Formula 1 which eliminated electrochemically inert binder shows a flat discharge curve for both CFx and CFy material. The energy density with this formulation is 1027 Wh/kg for CFx and 1060 Wh/kg for CFy, respectively. Although the CNT may aggregate in the electrode, it is shown that the framework formed by CNT is effectively conductive and robust.

Formula 2 which did not contain any conductive component in the middle layer shows a 0.1 V lower discharge voltage than Formula 1 for CFx. However, the discharge curve of two formulas overlay for CFy electrode, which implies that the sandwich-structure is playing a major role in improving the conductivity of the whole electrode.

In the expansion of initial discharge, the voltage delay is significantly alleviated for CFx material and it is completely removed for CFy material. Even for Formula 2 which does not have conductive additive component, comparable electrochemical results could be achieved, indicating that the sandwich-structure is a promising strategy in electrode-fabrication for CFx materials.

4 Conclusions

Li/CFx batteries are one of the most promising types of power sources by reasons of their high energy density, low self-discharge and high operating voltage. However, the low power drain rate resulted from the poor conductivity of CFx material limits their high-power application. In this work, we incorporated multi-walled carbon nanotubes in both active layer and current collector substrate of the CFx electrodes and studied the CNT as multiple components in the battery.

In this work, we took multiple steps to investigate the impact of CNT when playing different roles in Li/CFx batteries. First, to examine CNT as conductive additive in Li/CFx batteries, we studied the resistivity behaviour of CFx composite with different conductive additive. At 5 wt. %, CFx/super p shows 10 times higher of resistivity than that of CFx/CNT. At 10 wt. %, CFx/super p shows similar resistivity as CFx/ CNT. We proved that CNT are more effective in improving the conductivity of CFx system. To tackle the problem of CNT aggregation and improve the dispersion quality of CNT in CFx matrix, we studied the effect of physical ball-milling on dispersion status. Corresponding resistivity and electrochemical tests results were analysed. A time study was performed to get the optimal mixing status.

Second, we built CFx electrodes on CNT paper and compare the electrochemical performance of cells with CNT paper as current collector and those with conventional Al foil. The specific gravimetric capacity is increased by a factor of 2 at lower discharge current of 0.06 mA/cm^2 and improved by 100 mAh/g at other discharge currents tested compared with Al foil. Energy density is remarkably improved by 100-300 Wh/kg depending on discharge current and rate capability is enhanced. At 0.06/20/50 mA/cm^2, when the current is too high for the Al foil cell to sustain, the CNT substrate cell could give a capacity of 440 mAh/g. At the same pulse-discharge current, CNT cell maintains a higher voltage during the pulse, indicating higher electronic conductivity. A microcalorimetry study on the discharge pulse showed that the more heat was generated with Al foil as substrate than with CNT, which confirms the lower polarization of electrodes with CNT substrate. Furthermore, we were able to control the dimension of CFx-CNT electrodes and improved the energy density by reducing the mass on the CNT substrate. Last, we fabricated novel sandwich-structure electrode in which the active material was sandwiched between two layers of CNT. The sandwich structure relieved the initial voltage delay of CFx discharged, and high capacity and energy density were achieved.

In conclusion, we demonstrated that CNT have desirable benefits acting as multiple components of CFx electrodes, and employing CNT in Li/CFx batteries is worth further investigating from multiple perspectives.

Acknowledgements

The microcalorimetry studies were supported as part of the Center for Mesoscale Transport Properties, an Energy Frontier Research Center supported by the U.S. Department of Energy, Office of Science, Basic Energy Sciences, under award #DE-SC0012673. All other work was supported by the Northeastern Center for Chemical Energy Storage, an Energy Frontier Research Center funded by the U.S. DOE, BES under award No. DE-SC0001294, including matching support from NYSTAR-

NYSDED. Any opinions, findings, conclusions or recommendations expressed are those of the author(s) and do not necessarily reflect the views of the NYSDED.

Notes and references

‡ All CNT in the text refer to multi-walled carbon nanotubes.
*Super p Li is a type of conductive carbon black.

1. *US Pat.*, 3 536 532, 1970.
2. *US Pat.*, 3 700 502, 1972.
3. *US Pat.*, 4 271 242, 1981.
4. P. Lam and R. Yazami, *Journal of Power Sources*, 2006, 153, 354-359.
5. K. Guérin, J. P. Pinheiro, M. Dubois, Z. Fawal, F. Masin, R. Yazami and A. Hamwi, *Chemistry of Materials*, 2004, 16, 1786-1792.
6. M. J. Root, R. Dumas, R. Yazami and A. Hamwi, *Journal of The Electrochemical Society*, 2001, 148, A339-A345.
7. A. Zajac, P. Pelikán, J. Minár, J. Noga, M. Straka, P. Bañacký and S. Biskupič, *Journal of Solid State Chemistry*, 2000, 150, 286-293.
8. P. Pelikán, J. Noga and S. Biskupič, *Journal of Solid State Chemistry*, 2003, 174, 233-240.
9. T. Nakajima, R. Hagiwara, K. Moriya and N. Watanabe, *Journal of The Electrochemical Society*, 1986, 133, 1761-1766.
10. V. N. Mitkin, I. P. Asanov and L. N. Mazalov, *Journal of Structural Chemistry*, 2002, 43, 843-855.
11. L. Piraux, V. Bayot, J. P. Issi, M. S. Dresselhaus, M. Endo and T. Nakajima, *Physical Review B*, 1990, 41, 4961-4969.
12. S. L. di Vittorio, M. S. Dresselhaus, M. Endo and T. Nakajima, *Physical Review B*, 1991, 43, 12304-12315.
13. S. L. di Vittorio, M. S. Dresselhaus and G. Dresselhaus, *Journal of Materials Research*, 1993, 8, 1578-1585.
14. I. Palchan, M. Crespin, H. Estrade-Szwarckopf and B. Rousseau, *Chemical Physics Letters*, 1989, 157, 321-327.
15. S. S. Zhang, D. Foster, J. Wolfenstine and J. Read, *Journal of Power Sources*, 2009, 187, 233-237.
16. E. S. Takeuchi and R. A. Leising, *MRS Bulletin*, 2002, 27, 624-627.
17. H. Touhara, H. Fujimoto, N. Watanabe and A. Tressaud, *Solid State Ionics*, 1984, 14, 163-170.
18. N. Watanabe, T. Nakajima and R. Hagiwara, *Journal of Power Sources*, 1987, 20, 87-92.
19. T. Nakajima, R. Hagiwara, K. Moriya and N. Watanabe, *Journal of Power Sources*, 1987, 20, 93-98.
20. W. Tiedemann, *Journal of The Electrochemical Society*, 1974, 121, 1308-1311.
21. H. F. Hunger and J. E. Ellison, *Journal of The Electrochemical Society*, 1975, 122, 1288-1291.
22. M. S. Whittingham, *Journal of The Electrochemical Society*, 1975, 122, 526-527.
23. N. Watanabe, R. Hagiwara, T. Nakajima, H. Touhara and K. Ueno, *Electrochimica Acta*, 1982, 27, 1615-1619.
24. M. Dubois, K. Guerin, W. Zhang, Y. Ahmad, A. Hamwi, Z. Fawal, H. Kharbache and F. Masin, *Electrochimica Acta*, 2012, 59, 485-491.
25. W. Zhang, M. Dubois, K. Guerin, P. Bonnet, H. Kharbache, F. Masin, A. P. Kharitonov and A. Hamwi, *Physical Chemistry Chemical Physics*, 2010, 12, 1388-1398.
26. S. Davis, E. S. Takeuchi, W. Tiedemann and J. Newman, *Journal of the Electrochemical Society*, 2007, 154, A477-A480.
27. S. Davis, E. S. Takeuchi, W. Tiedemann and J. Newman, *Journal of the Electrochemical Society*, 2008, 155, A24-A28.
28. W. Liu, H. Li, J.-Y. Xie and Z.-W. Fu, *ACS Applied Materials & Interfaces*, 2014, 6, 2209-2212.
29. C. F. Holmes and B. B. Owens, in *Wiley Encyclopedia of Biomedical Engineering*, John Wiley & Sons, Inc., 2006.
30. B. F. Antonioli G, Consiglio F, et al, *Minerva Medica*, 1973, 64.
31. C. F. Holmes, *Journal of Power Sources*, 2001, 97–98, 739-741.
32. W. Greatbatch, C. F. Holmes, E. S. Takeuchi and S. J. Ebel, *Pace-Pacing and Clinical Electrophysiology*, 1996, 19, 1836-1840.
33. C. F. Holmes, *Journal of Power Sources*, 1997, 65, xv-xx.
34. W. C. W. Greatbatch, *New England Research and Eng. Meet.*, 1959, 1.
35. B. B. Owens, *Batteries for implantable biomedical devices*, Plenum Press, 1986.
36. K. Nishio, in *Encyclopedia of Electrochemical Power Sources*, ed. J. Garche, Elsevier, Amsterdam, 2009, DOI: http://dx.doi.org/10.1016/B978-044452745-5.00115-5, pp. 83-92.
37. D. O. B. A.J. Cuesta, presented in part at the Power Sources for Biomedical Implantable Applications and Ambient Temperature Lithium Batteries, Princeton, NJ, 1980.
38. C. Holmes, *ECS Transactions*, 2007, 6, 1-7.
39. R. J. Brodd, K. R. Bullock, R. A. Leising, R. L. Middaugh, J. R. Miller and E. Takeuchi, *Journal of the Electrochemical Society*, 2004, 151, K1-K11.
40. A. Skunidin, S. Fateev and T. Kulova, *Advanced Batteries and Accumulators*, 2001, 2.
41. V. S. Mallela, V. Ilankumaran and N. Rao, *Indian Pacing and Electrophysiology Journal*, 2004, 4, 201-212.
42. *U.S. Pat.*, 0081545, 2009.
43. D. Linden and T. B. Reddy, *Handbook of batteries*, McGraw-Hill, 2002.
44. D. C. Bock, A. C. Marschilok, K. J. Takeuchi and E. S. Takeuchi, *Electrochimica Acta*, 2012, 84, 155-164.
45. K. Chen, D. R. Merritt, W. G. Howard, C. L. Schmidt and P. M. Skarstad, *Journal of Power Sources*, 2006, 162, 837-840.
46. H. Gan, R. S. Rubino and E. S. Takeuchi, *Journal of Power Sources*, 2005, 146, 101-106.
47. D. D. Pagoria, S. A. Megahed, J. L. Lautzenhiser and R. J. Ekern, 1992.
48. M.-L. Chan, *Journal of Power Sources*, 1999, 80, 273-277.
49. E. I. Eweka, C. O. Giwa, G. O. Mepsted, K. Green and D. Scattergood, *Journal of Power Sources*, 2006, 162, 841-846.
50. A. G. Ritchie, C. O. Giwa, P. G. Bowles, J. Burgess, E. Eweka and A. Gilmour, *Journal of Power Sources*, 2001, 96, 180-183.
51. C. O. Giwa, A. G. Ritchie, P. G. Bowles and E. L. Price, Cherry Hill, NJ, USA, 2000.
52. C. O. Giwa, A. G. Ritchie, E. I. Eweka, P. G. Bowles and A. Gilmour, Fort Lauderdale, Florida, USA, 2003.
53. S. Zhang, D. Foster, J. Wolfenstine and J. Read, *Fluorinate Carbon Composite Cathode for a High Energy Lithium Battery*, US Army RDECOM, 2011.
54. T. B. R. David Linden, *Handbook of Batteries*, McGraw-Hill, New York, 3rd edn., 2001.
55. R. Hagiwara, T. Nakajima and N. Watanabe, *Journal of The Electrochemical Society*, 1988, 135, 2128-2133.
56. R. Yazami, A. Hamwi, K. Guérin, Y. Ozawa, M. Dubois, J. Giraudet and F. Masin, *Electrochemistry Communications*, 2007, 9, 1850-1855.
57. S. S. Zhang, D. Foster and J. Read, *Journal of Power Sources*, 2009, 191, 648-652.
58. S. S. Zhang, D. Foster and J. Read, *Journal of Power Sources*, 2009, 188, 601-605.
59. Q. Zhang, S. D'Astorg, P. Xiao, X. Zhang and L. Lu, *Journal of Power Sources*, 2010, 195, 2914-2917.
60. H. Groult, C. M. Julien, A. Bahloul, S. Leclerc, E. Briot and A. Mauger, *Electrochemistry Communications*, 2011, 13, 1074-1076.
61. G. Nagasubramanian and B. Sanchez, *Journal of Power Sources*, 2007, 165, 630-634.
62. E. Rangasamy, J. Li, G. Sahu, N. Dudney and C. Liang, *Journal of the American Chemical Society*, 2014, 136, 6874-6877.
63. R. Jayasinghe, A. K. Thapa, R. R. Dharmasena, T. Q. Nguyen, B. K. Pradhan, H. S. Paudel, J. B. Jasinski, A. Sherehiy, M. Yoshio and G. U. Sumanasekera, *Journal of Power Sources*, 2014, 253, 404-411.
64. D. Damien, P. M. Sudeep, T. N. Narayanan, M. R. Anantharaman, P. M. Ajayan and M. M. Shaijumon, *RSC Adv.*, 2013, 3, 25702-25706.
65. M. A. Reddy, B. Breitung and M. Fichtner, *ACS Applied Materials & Interfaces*, 2013, 5, 11207-11211.
66. W. Yang, Y. Dai, S. Cai, Y. Zheng, W. Wen, K. Wang, Y. Feng and J. Xie, *Journal of Power Sources*, 2014, 255, 37-42.
67. B. Marinho, M. Ghislandi, E. Tkalya, C. E. Koning and G. de With, *Powder Technology*, 2012, 221, 351-358.

68. S. Berber, Y.-K. Kwon and D. Tománek, *Physical Review Letters*, 2000, 84, 4613-4616.
69. Z. Zhang, J. Peng and H. Zhang, *Applied Physics Letters*, 2001, 79, 3515-3517.
70. R. H. Baughman, A. A. Zakhidov and W. A. de Heer, *Science*, 2002, 297, 787-792.
71. H. Dai, *Surface Science*, 2002, 500, 218-241.
72. X. Zhang, T. V. Sreekumar, T. Liu and S. Kumar, *The Journal of Physical Chemistry B*, 2004, 108, 16435-16440.
73. E. M. Jin, B. Jin, K.-H. Park, H.-B. Gu, G.-C. Park and K.-W. Kim, *Journal of Nanoscience and Nanotechnology*, 2008, 8, 5057-5061.
74. H. Gwon, J. Hong, H. Kim, D.-H. Seo, S. Jeon and K. Kang, *Energy & Environmental Science*, 2014, 7, 538-551.
75. B. J. Landi, M. J. Ganter, C. D. Cress, R. A. DiLeo and R. P. Raffaelle, *Energy & Environmental Science*, 2009, 2, 638-654.
76. S. W. Lee, N. Yabuuchi, B. M. Gallant, S. Chen, B.-S. Kim, P. T. Hammond and Y. Shao-Horn, *Nat Nano*, 2010, 5, 531-537.
77. J. Wang and M. Musameh, *Analytical Chemistry*, 2003, 75, 2075-2079.
78. H.-Z. Geng, K. K. Kim, K. P. So, Y. S. Lee, Y. Chang and Y. H. Lee, *Journal of the American Chemical Society*, 2007, 129, 7758-7759.
79. J. W. Jo, J. W. Jung, J. U. Lee and W. H. Jo, *ACS Nano*, 2010, 4, 5382-5388.
80. Z. Wu, Z. Chen, X. Du, J. M. Logan, J. Sippel, M. Nikolou, K. Kamaras, J. R. Reynolds, D. B. Tanner, A. F. Hebard and A. G. Rinzler, *Science*, 2004, 305, 1273-1276.
81. G. Xu, Q. Zhang, W. Zhou, J. Huang and F. Wei, *Appl. Phys. A*, 2008, 92, 531-539.
82. Á. Kukovecz, R. Smajda, Z. Kónya and I. Kiricsi, *Carbon*, 2007, 45, 1696-1698.
83. D. Wang, P. Song, C. Liu, W. Wu and S. Fan, *Nanotechnology*, 2008, 19.
84. R. L. D. Whitby, T. Fukuda, T. Maekawa, S. L. James and S. V. Mikhalovsky, *Carbon*, 2008, 46, 949-956.
85. K. Lin, Y. Xu, G. He and X. Wang, *Materials Chemistry and Physics*, 2006, 99, 190-196.
86. M.-S. Park, S. A. Needham, G.-X. Wang, Y.-M. Kang, J.-S. Park, S.-X. Dou and H.-K. Liu, *Chemistry of Materials*, 2007, 19, 2406-2410.
87. G. Lota, B. Grzyb, H. Machnikowska, J. Machnikowski and E. Frackowiak, *Chemical Physics Letters*, 2005, 404, 53-58.
88. S. W. Lee, B.-S. Kim, S. Chen, Y. Shao-Horn and P. T. Hammond, *Journal of the American Chemical Society*, 2008, 131, 671-679.
89. H. R. Byon, B. M. Gallant, S. W. Lee and Y. Shao-Horn, *Advanced Functional Materials*, 2013, 23, 1037-1045.
90. T. Le Gall, K. H. Reiman, M. C. Grossel and J. R. Owen, *Journal of Power Sources*, 2003, 119, 316-320.
91. K. Kendall, *Journal of Physics D-Applied Physics*, 1990, 23, 1329-1331.
92. L. E. E. R.L. Powell, *American Institute of Physics Handbook*, 1972.
93. N. Grossiord, J. Loos, O. Regev and C. E. Koning, *Chemistry of Materials*, 2006, 18, 1089-1099.
94. J. Li, P. C. Ma, W. S. Chow, C. K. To, B. Z. Tang and J. K. Kim, *Advanced Functional Materials*, 2007, 17, 3207-3215.
95. Y. S. Song and J. R. Youn, *Carbon*, 2005, 43, 1378-1385.
96. E. S. Choi, J. S. Brooks, D. L. Eaton, M. S. Al-Haik, M. Y. Hussaini, H. Garmestani, D. Li and K. Dahmen, *Journal of Applied Physics*, 2003, 94, 6034-6039.
97. V. Georgakilas, K. Kordatos, M. Prato, D. M. Guldi, M. Holzinger and A. Hirsch, *Journal of the American Chemical Society*, 2002, 124, 760-761.
98. R. Ramasubramaniam, J. Chen and H. Y. Liu, *Applied Physics Letters*, 2003, 83, 2928-2930.
99. N. Hamada, S.-i. Sawada and A. Oshiyama, *Physical Review Letters*, 1992, 68, 1579-1581.
100. P. L. McEuen, M. Bockrath, D. H. Cobden and J. G. Lu, *Microelectronic Engineering*, 1999, 47, 417-420.
101. E. Raymundo-Piñero, V. Khomenko, E. Frackowiak and F. Béguin, *Journal of The Electrochemical Society*, 2005, 152, A229-A235.
102. W. Guoping, Z. Qingtang, Y. Zuolong and Q. MeiZheng, *Solid State Ionics*, 2008, 179, 263-268.
103. Y. Li, Y. Chen, W. Feng, F. Ding and X. Liu, *Journal of Power Sources*, 2011, 196, 2246-2250.
104. X.-L. Xie, Y.-W. Mai and X.-P. Zhou, *Materials Science and Engineering: R: Reports*, 2005, 49, 89-112.
105. Y. A. Kim, T. Hayashi, Y. Fukai, M. Endo, T. Yanagisawa and M. S. Dresselhaus, *Chemical Physics Letters*, 2002, 355, 279-284.
106. N. Pierard, A. Fonseca, Z. Konya, I. Willems, G. Van Tendeloo and J. B.Nagy, *Chemical Physics Letters*, 2001, 335, 1-8.
107. J. Hilding, E. Grulke, Z. George Zhang and F. Lockwood, *Journal of Dispersion Science & Technology*, 2003, 24, 1.
108. Y. J. Noh, S. Y. Pak, S. H. Hwang, J. Y. Hwang, S. Y. Kim and J. R. Youn, *Composites Science and Technology*, 2013, 89, 29-37.
109. D. Qian, E. C. Dickey, R. Andrews and T. Rantell, *Applied Physics Letters*, 2000, 76, 2868-2870.
110. J. Sandler, M. S. P. Shaffer, T. Prasse, W. Bauhofer, K. Schulte and A. H. Windle, *Polymer*, 1999, 40, 5967-5971.
111. H. Wang, W. Zhou, D. L. Ho, K. I. Winey, J. E. Fischer, C. J. Glinka and E. K. Hobbie, *Nano Letters*, 2004, 4, 1789-1793.
112. A. G. Ryabenko, T. V. Dorofeeva and G. I. Zvereva, *Carbon*, 2004, 42, 1523-1535.
113. M. F. Islam, E. Rojas, D. M. Bergey, A. T. Johnson and A. G. Yodh, *Nano Letters*, 2003, 3, 269-273.
114. E. A. Whitsitt and A. R. Barron, *Nano Letters*, 2003, 3, 775-778.
115. J. Yu, N. Grossiord, C. E. Koning and J. Loos, *Carbon*, 2007, 45, 618-623.
116. R. Rastogi, R. Kaushal, S. K. Tripathi, A. L. Sharma, I. Kaur and L. M. Bharadwaj, *Journal of Colloid and Interface Science*, 2008, 328, 421-428.
117. H. Huang, H. Kajiura, A. Yamada and M. Ata, *Chemical Physics Letters*, 2002, 356, 567-572.
118. K. Esumi, M. Ishigami, A. Nakajima, K. Sawada and H. Honda, *Carbon*, 1996, 34, 279-281.
119. D. B. Mawhinney, V. Naumenko, A. Kuznetsova, J. T. Yates, J. Liu and R. E. Smalley, *Journal of the American Chemical Society*, 2000, 122, 2383-2384.
120. Q. Chen, L. Dai, M. Gao, S. Huang and A. Mau, *The Journal of Physical Chemistry B*, 2000, 105, 618-622.
121. J. L. Bahr and J. M. Tour, *Journal of Materials Chemistry*, 2002, 12, 1952-1958.
122. J. E. Riggs, Z. Guo, D. L. Carroll and Y.-P. Sun, *Journal of the American Chemical Society*, 2000, 122, 5879-5880.
123. L. Cao, H. Chen, M. Wang, J. Sun, X. Zhang and F. Kong, *The Journal of Physical Chemistry B*, 2002, 106, 8971-8975.
124. Y. Lin, B. Zhou, K. A. Shiral Fernando, P. Liu, L. F. Allard and Y.-P. Sun, *Macromolecules*, 2003, 36, 7199-7204.
125. D. E. Hill, Y. Lin, A. M. Rao, L. F. Allard and Y.-P. Sun, *Macromolecules*, 2002, 35, 9466-9471.
126. K. L. Lu, R. M. Lago, Y. K. Chen, M. L. H. Green, P. J. F. Harris and S. C. Tsang, *Carbon*, 1996, 34, 814-816.
127. Y. B. Li, B. Q. Wei, J. Liang, Q. Yu and D. H. Wu, *Carbon*, 1999, 37, 493-497.
128. J. W. Cho, J. W. Kim, Y. C. Jung and N. S. Goo, *Macromolecular Rapid Communications*, 2005, 26, 412-416.
129. J. Read, E. Collins, B. Piekarski and S. Zhang, *Journal of the Electrochemical Society*, 2011, 158, A504-A510.
130. A. Hamwi, *Journal of Physics and Chemistry of Solids*, 1996, 57, 677-688.